Theoret. Chim. Acta (Berl.) 55, 133–151 (1980)

THEORETICA CHIMICA ACTA
© by Springer-Verlag 1980

# Binding/Antibinding Analyses for Diatomic Interactions $H_2^+$ System

Toshikatsu Koga, Tsutomu Nishijima, and Mutsuo Morita

Department of Industrial Chemistry, Muroran Institute of Technology, Muroran, 050 Japan

The region-functional concept of electron density has been quantitatively examined for $1s\sigma_g$, $2p\sigma_u$, $2p\pi_u$, and $3d\pi_g$ states of $H_2^+$ system on the basis of Berlin diagram which divides the three-dimensional molecular space into binding and antibinding regions. The electronic charge, Hellmann–Feynman (H–F) force, and stabilization energy of the system are partitioned into the binding and antibinding contributions by the regional integrations.

Dynamic behaviors of the electron density (i.e. electron-cloud preceding and following) during the interaction processes are also clarified using the centers of electron density and force density.

Differences in attractive and repulsive, and $\sigma$- and $\pi$-type interactions are discussed from the force and density point of view.

**Key words:** Berlin diagram – Hellmann–Feynman force – $H_2^+$ system.

## 1. Introduction

Because of its direct relationship to experiment, it is reasonable to adopt the electron density for the description of a system in theoretical chemistry [1]. The electron density is a well-defined physical quantity and permits a direct physical picture and interpretation of the system, though the wavefunction itself does not. The physical simplicity of the electron density is further developed by the use of the Hellmann–Feynman (H–F) theorem [2]. It connects the force acting on a nucleus and the electron density of the system in an intuitive and yet quantitative manner [3].

Based on this simple and exact relationship between the force and the density, Berlin derived the region-functional concept of the electron density for diatomic

0040-5744/80/0055/0133/$04.00

molecules [4]. He showed that the molecular space can be divided into the binding and antibinding regions (Berlin diagram); the electron density in the binding region tends to draw the nuclei together while the density in the antibinding region tends to pull them apart. Recently, Koga et al. have given an unambiguous generalization of Berlin's concept for polyatomic molecules [5], in which analogously to diatomic cases, the space around a molecule has been shown to be separable into the accelerating and registing regions with respect to a given internal (symmetry or normal) coordinate (generalized Berlin diagram).

These diagrams have provided an explicit foundation for the density guiding rule for nuclear rearrangement processes [6]. The Berlin diagram has also been referred to rationalize the density accumulation in the bond region of stable (covalent) molecules [7]. However, the discussion has remained rather qualitative and static. So far as we know, the quantitative results reported are only the amounts of the binding and antibinding charges for several ground-state diatomic molecules at their equilibrium bond lengths [8].

A purpose of this paper is to examine the binding and antibinding contributions of electron density for the processes of attractive and repulsive interactions in a quantitative manner. The present study is also the first step towards the quantitative application of the generalized Berlin diagram. In order to avoid possible errors, we have chosen one-electron $H_2^+$ system for which the exact analytical wavefunctions are known in a series expansion form [9]. Since the system is a prototype of homonuclear diatonics, its analysis would give some insight into the nature of covalent bonds without any approximations[1]. It should be stressed that in the force and density approach, all the required quantity is the electron density. Moreover, integration of the force (i.e. the integrated H–F theorem [11]) enables us to relate directly the density behavior with the energy of the system. This is not true when one stands on the traditional energetic side (compare with e.g. [10, 12]). In the following, we quantitatively examine the regional contributions of the electron density[2] in terms of the amount of electronic charge, H–F force, and stabilization energy of the system for the ground and three excited states. The center of electron density (CED) and the center of force density (CFD) are introduced to clarify a way of the density distribution in each region, e.g. whether it is delocalized or contracted. They are also measures for the electron-cloud preceding and (incomplete) following [6].

## 2. Theoretical Ground

On the basis of the H–F theorem [2], the interatomic force $F$ in diatomic systems is given by

$$F = -\int f(\boldsymbol{r}; R)\rho(\boldsymbol{r}; R)\, d\boldsymbol{r} + Z_A Z_{A'}/R^2, \tag{1}$$

[1] An energetic analysis of $H_2^+$ system has been given in detail by Ruedenberg et al. [10].

[2] Politzer et al. [13] have used similar regional-integration technique to define atomic charges in linear molecules based on the electron-count method [16]. Their definition has been shown to be less basis-dependent than the Mulliken population analysis [13–15].

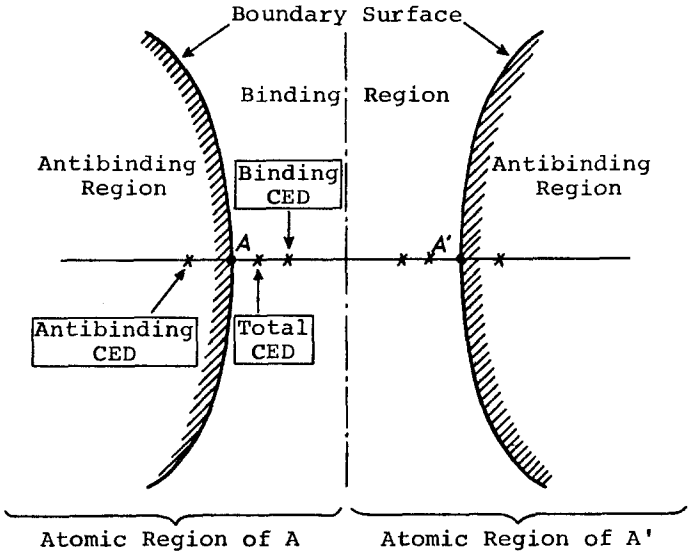


**Fig. 1.** Schematic representation of the binding–antibinding regions and atomic regions for homonuclear diatomics. Typical situations of the total, binding, and antibinding CED's are also given for attractive cases

where $R$ is the internuclear distance, $\rho(\boldsymbol{r}; R)$ the electron density, and $f(\boldsymbol{r}; R)$ the force operator; $f = (Z_A \cos\theta_A/r_A^2 + Z_{A'} \cos\theta_{A'}/r_{A'}^2)/2$, with $r_A$ and $\theta_A$ being polar coordinates measured from nucleus $A$ whose charge is $Z_A$. Since the electron density $\rho$ is non-negative, the first term in Eq. (1) gives attractive (binding) force if $f > 0$ and repulsive (antibinding) force if $f < 0$. Thus Berlin [4] divided the space of the electronic charge distribution into binding ($f > 0$) region and antibinding ($f < 0$) region (Berlin diagram, see Fig. 1).

The contribution of the electron density to the diatomic binding is regionally distinguished. Then physical quantity $G$ which depends only on the electron density $\rho$ can be partitioned into the two contributions by carrying out the integration over each of these regions;

$$\bar{G}_D(R) = \int_D G(\boldsymbol{r}; R)\rho(\boldsymbol{r}; R)\, d\boldsymbol{r}, \tag{2}$$

where $\int_D d\boldsymbol{r}$ means the integration over the binding or antibinding region. For the amount of electronic charge $G = 1$ and for the electronic part of the H–F force $G = f$. Integration of the partitioned forces then gives the regional contribution of the electron density to the stabilization energy;

$$\Delta E_D(R) = \int_\infty^R \bar{f}_D(R)\, dR. \tag{3}$$

The center of electron density (CED) is defined with respect to atomic density. For the homonuclear case, the plane which perpendicularly bisects the internuclear

axis separates the molecular space into two atomic regions (Fig. 1). Then the CED is given by

$$\bar{r}_A(R) = \int_A r\rho(r; R)\, dr \Big/ \int_A \rho(r; R)\, dr, \tag{4}$$

where $\int_A dr$ means the integration over the atomic region. This definition is originally due to Politzer [13*b*]. The CED in Eq. (4) is hereafter referred to as total CED, and is further decomposed into binding and antibinding CED's by the regional integration. The shifts of these centers from their separated atom (SA) values[3] provide quantitative measures for the dynamic behavior of the electron density such as the electron-cloud preceding and following [6]. The component CED's also introduce the concept of contraction and delocalization of the partitioned densities. All the CED's lie on the internuclear axis of symmetry of the system. In Fig. 1, we have shown their typical situations for attractive interactions.

The center of force density (CFD) is similarly defined by substituting the norm of the force density $|f\rho|(=|f|\rho)$ for the electron density $\rho$ in Eq. (4). Though the norm is used to avoid the divergence of the total CFD in the case of zero electronic force (e.g. $R\to\infty$), it has no effect on the component CFD's. The force density represents the actual contribution of the electron density to the binding of the system. Due to the weighting factor $f$, it is more localized around the nuclei and the internuclear axis than the electron density itself. We will see in the next section that the behaviors of the CED's and CFD's in the interaction processes are nearly parallel.

## 3. Results and Discussion

### *3.1. $1s\sigma_g$ State*

The results of the binding and antibinding analysis for the $1s\sigma_g$ ground state are given in Figs. 2–4*a*. As does the stabilization energy in Fig. 2*b*, the total H–F force in Fig. 2*a* correctly reproduces the known equilibrium bond distance $R_e = 2.00$ a.u.[4]; it is attractive for $R > R_e$ with maximum attraction at $R \simeq 3.3$ a.u. and repulsive for $R < R_e$. We see in Fig. 2 that the total force and stabilization energy result from a sensitive balance between the electronic part (attractive and stabilizing) and the nuclear part (repulsive and destabilizing). Of the two components of the electronic force (Fig. 2*a*), the binding force monotonously increases its attraction from the SA value. The force works to stabilize the system (Fig. 2*b*). On the other hand, the antibinding force decreases its repulsion for $R \geqslant 1.9$ a.u. (minimum at $R \simeq 4.0$ a.u.) when compared with its SA value. It also

[3] In the SA limit ($R\to\infty$), the total CED and CFD are on the nucleus, and the component CED's and CFD's are on the opposite side each other with the same distance from the nucleus. This is due to that the boundary surfaces are reduced to the two perpendicular planes passing through the nuclei.

[4] Most accurate theoretical value seems to be $R_e = 1.9971933198$ a.u. [17].

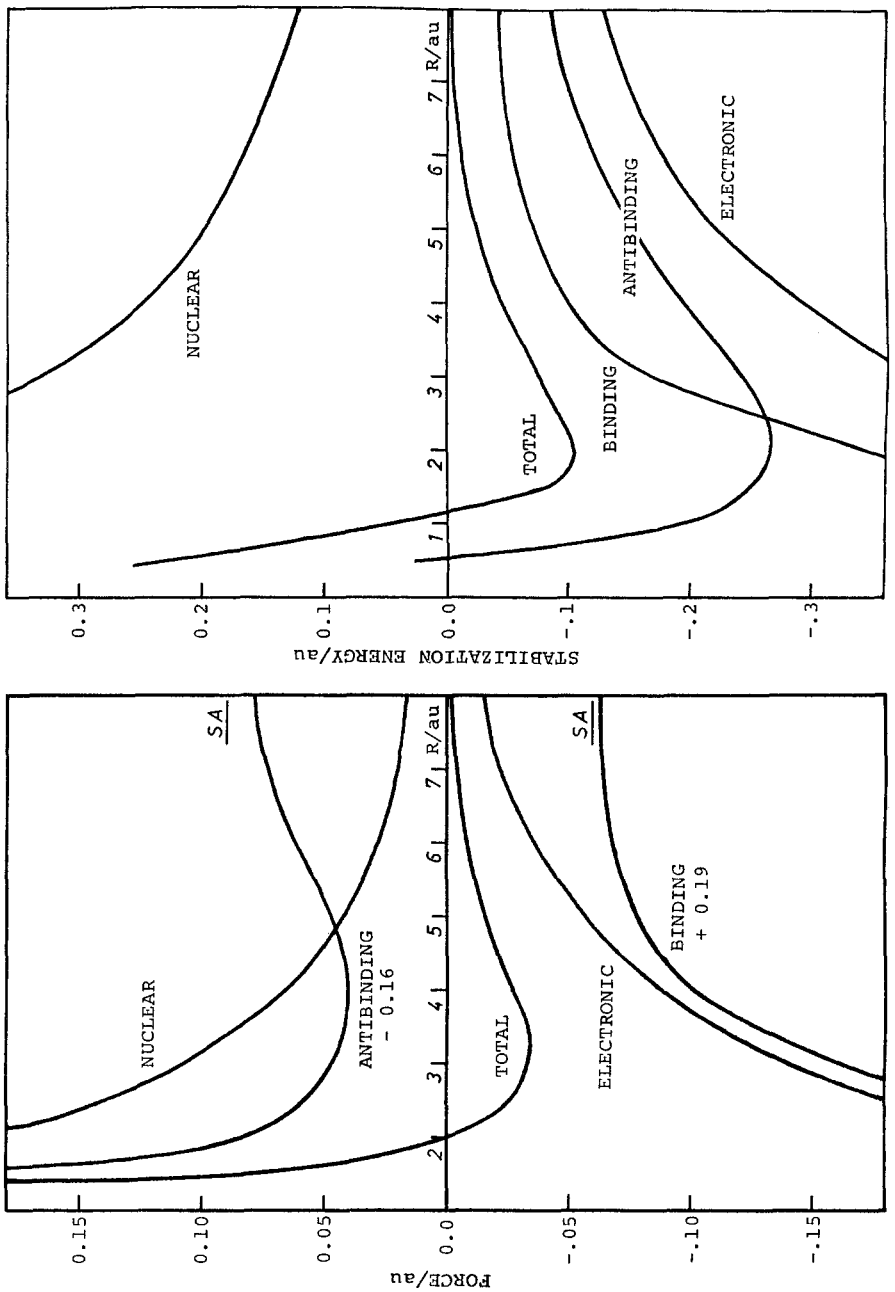


**Fig. 2.** $1s\sigma_g$ State. (a) Partitioning of the H–F force. Negative and positive values correspond to attraction and repulsion, respectively. The SA values are −0.25 and 0.25 a.u. for the binding and antibinding forces. (b) Partitioning of the stabilization energy. Negative and positive values correspond to stabilization and destabilization, respectively

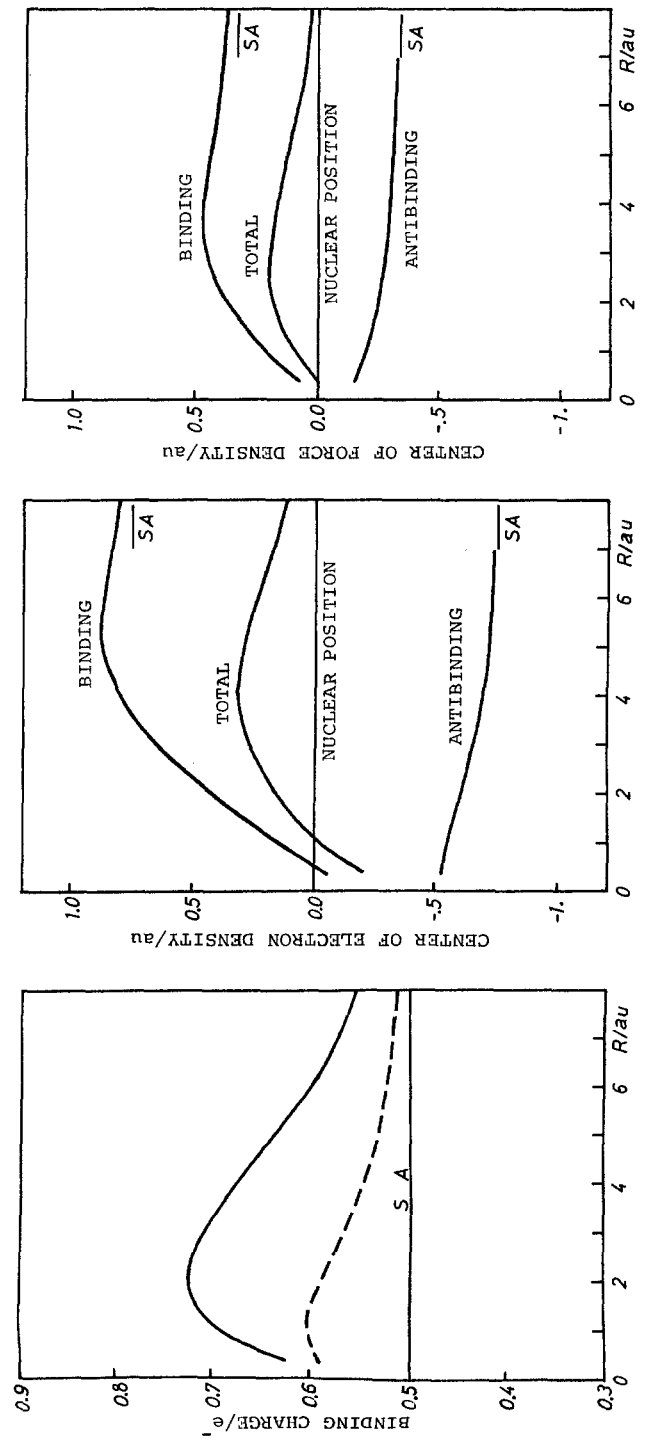


**Fig. 3.** $1s\sigma_g$ State. (a) Binding charge. The broken line shows the binding charge obtained from the superposed atomic density. The SA value is $0.5\,e^-$. (b) CED's. Positive value means the inside of the nucleus. The SA values are 0.0, 0.75, and −0.75 au for the total, binding, and antibinding CED's, respectively. (c) CFD's. The SA values are 0.0, 1/3, and −1/3 au for the total, binding, and antibinding CFD's, respectively

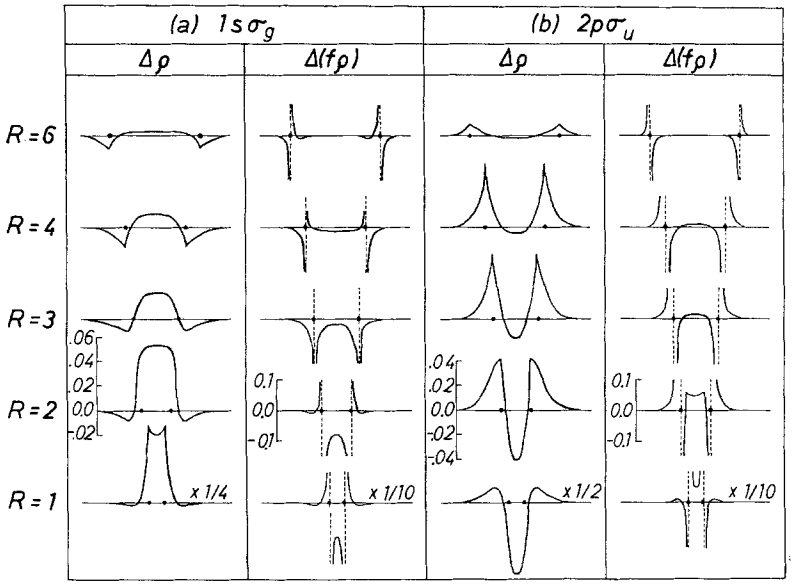


**Fig. 4.** Density difference $\Delta\rho$ and force density difference $\Delta(f\rho)$ along the internuclear axis. The reference density $\rho_0$ and force density $(f\rho)_0$ have been chosen to $\rho_0=(\rho_A+\rho_{A'})/2$ and $(f\rho)_0=(f_A\rho_A+f_{A'}\rho_{A'})/2$, respectively. (a) $1s\sigma_g$ State. (b) $2p\sigma_u$ State

contributes to the stabilization. Thus both of the binding and antibinding contributions are cooperative for the bond formation. Moreover, it is remarkable in Fig. 2*a* and *b* that the antibinding and total curves are nearly parallel. This suggests that the density reorganization in the antibinding region would play a more important role than the usually recognized one. Indeed, Fig. 2*b* shows that the antibinding contribution is larger than the binding one for $R \gtrsim 2.5$ a.u. This point will be discussed later.

The origin of these attraction and stabilization is the transfer of the electron density from the antibinding region. In Fig. 4*a*, profile of such charge migration is depicted by the density difference $\Delta\rho$ along the internuclear axis. The charge transfer first comes out as an inward polarization of the density near the nuclei and then as a density accumulation in the center of the binding region. This has been already found for several systems [18, 19]. Also given in Fig. 4*a* is the force density difference $\Delta(f\rho)$, which shows that for large separations (e.g. $R \geq 4$ a.u.) the decrease in the antibinding density is a dominant origin of the attractive force, while the increase in the binding density is for shorter distances (e.g. $R \leq 3$ a.u.)[5]. In Fig. 3*a*, the amount of the binding charge is given against $R$. It gradually increases as $R$ lowers to $R_e$, in accordance with the ordinary concept of the covalent bond formation. At the equilibrium distance, the binding charge is $0.723\,e^-$ and interestingly it is almost maximum at this point. This is also true when the binding

[5] At long-range limit, these two contributions are the same in magnitude, since the decrease and increase of the electron density are symmetric with respect to the nucleus [20].

charge from the superposed atomic density (dashed line in Fig. 3*a*) is chosen as the reference instead of the SA value.

These density reorganizations are the electron-cloud preceding [6] which accelerates the bond formation. In Fig. 3*b*, the total CED shifts inwardly for $R \geq 1$ a.u. and shows that the electron-cloud preceding occurs even at $R = R_e$ by 0.138 a.u. The maximum preceding (0.137 a.u.) is found at $R \simeq 4.0$ a.u. The binding CED shifts inwardly for $R > 3.7$ a.u. and outwardly for $R < 3.7$ a.u. from the SA value (0.75 a.u.), meaning that the binding density is first delocalized over the region but is rather contracted near the nuclei for shorter distance. The antibinding CED shows an inward shift (i.e. contraction) throughout the process and is responsible for the inward shift of the total CED at small separations. The CFD curves given in Fig. 3*c* are similar to the CED's in their behaviors. A difference is seen for the total and binding curves in which the CFD's predict a longer continuation of the electron-cloud preceding.

As mentioned before, the contributions of the partitioned densities to the stabilization energy of the system are different. Since the amount of the charge decreased in the antibinding region is exactly equal to that increased in the binding region, a manner of these charge distributions may be responsible for the different energetic contributions. Of the two regional density reorganizations in the $1s\sigma_g$ state, the present analysis suggests that the decrease in the contracted antibinding density is more effective to the binding than the increase in the delocalized binding density, though they occur simultaneously and are cooperative.

### *3.2. $2p\sigma_u$ State*

The results for the $2p\sigma_u$ state are given in Figs. 4*b*–6. Differences in the force and density origins for the attractive ($1s\sigma_g$) and repulsive ($2p\sigma_u$) states are of our main interests. The total force in Fig. 5*a* is repulsive throughout the process and no stable molecule is found in this state. The stabilization energy shows the same result (Fig. 5*b*). When compared with the attractive $1s\sigma_g$ state, the repulsion (and destabilization) is ascribed to both the binding and antibinding parts. For the range examined, the increase in the binding force is rather small and the force is nearly constant for $7 > R > 3$ a.u. Though it slightly decreases at a large separation ($R > 7$ a.u.), the antibinding force monotonously increases its repulsion for $7 > R > 2$ a.u. As a result, even the electronic force changes from attractive to repuslive at $R \simeq 3.3$ a.u. In Fig. 5*b*, the stabilization energy due to the binding part is not so large and the contribution of the antibinding part is barely stabilizing ($R > 4.9$ a.u.) or destabilizing ($R < 4.9$ a.u.). The curves in Fig. 5 show drastic changes for $R < 2$ a.u. This may be attributed to the $2p\sigma$(He) character of the electron density at this distance (see also Fig. 4*b*).

These repulsion and destabilization are the result of the electron-cloud following [6]. Contrary to the electron-cloud preceding observed in the $1s\sigma_g$ state, it appears as the flow of the electron density from the binding to the antibinding region and as the outward shift of the CED's and CFD's (Figs. 4*b* and 6). The $\Delta\rho$ in Fig. 4*b* shows that the binding density decreases at the center of the two nuclei

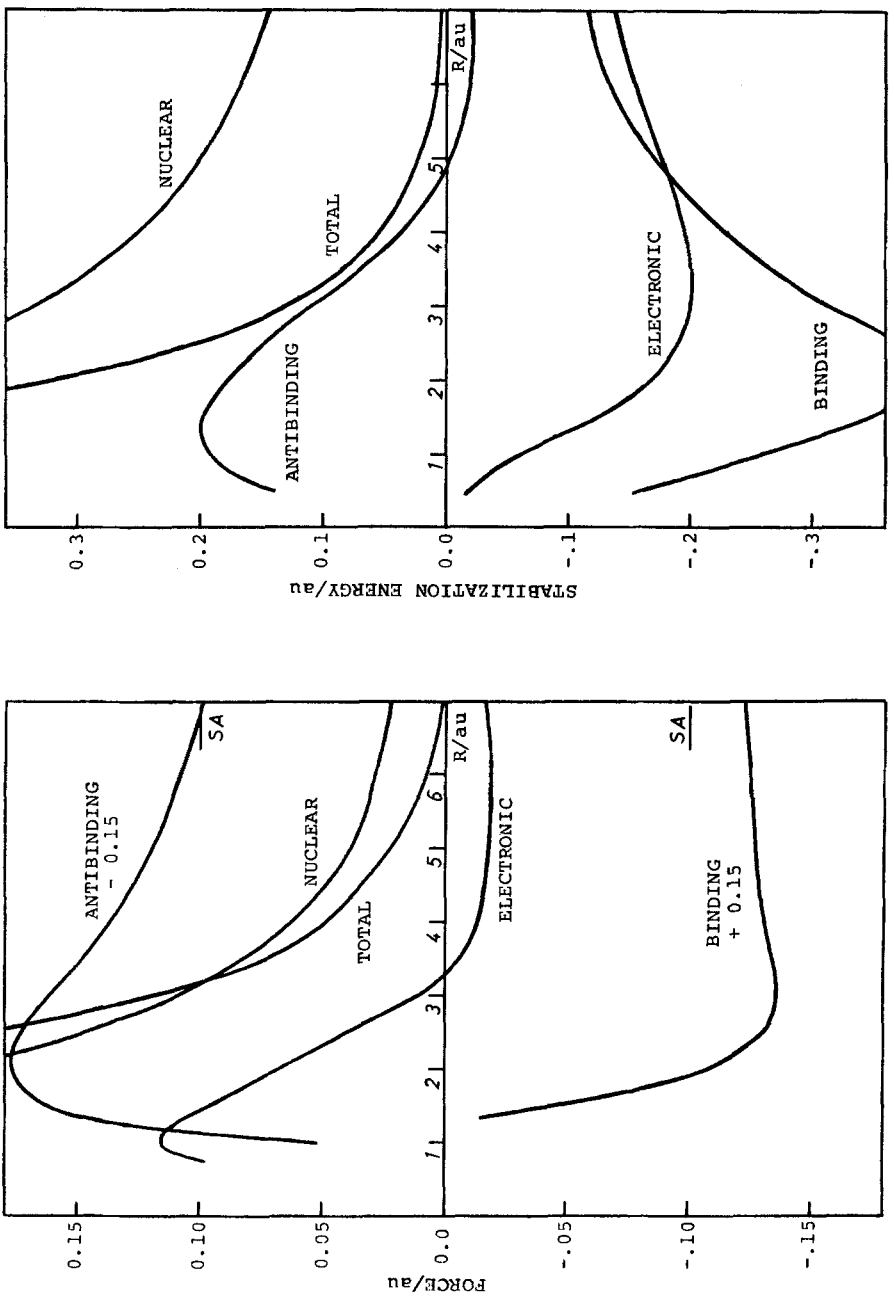


**Fig. 5.** $2p\sigma_u$ State. See the captions of Fig. 2

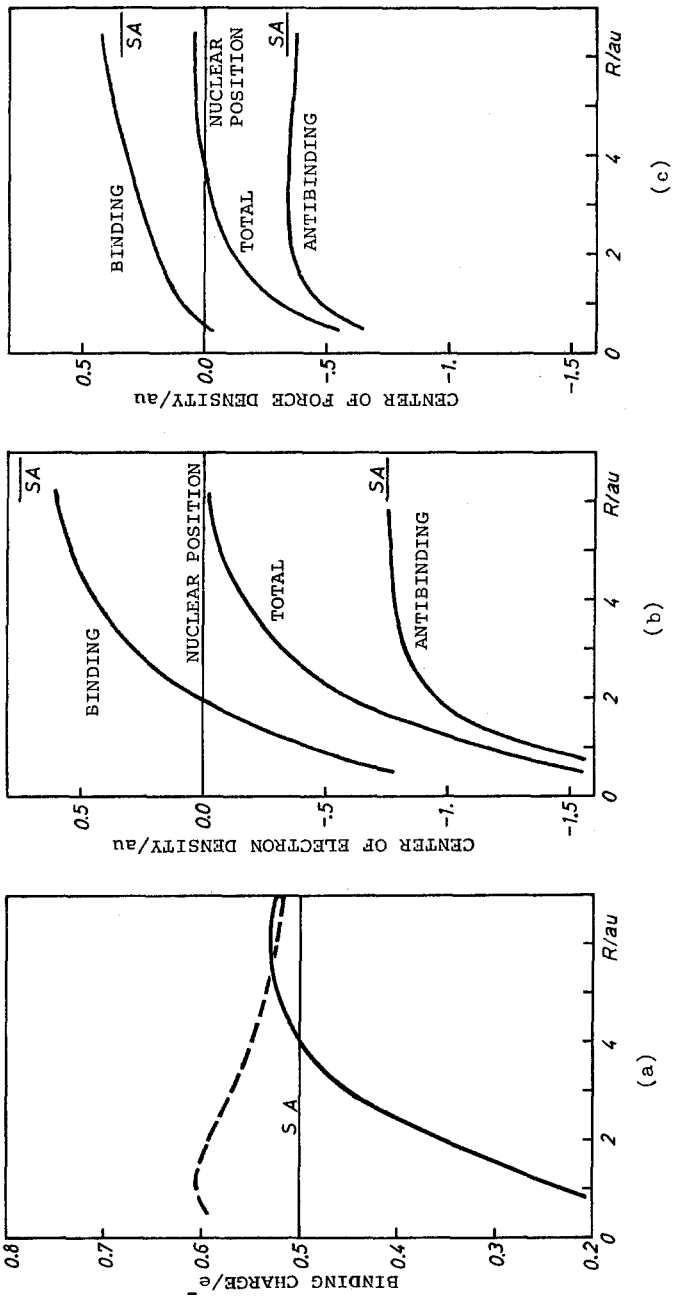


**Fig. 6.** $2p\sigma_u$ State. See the captions of Fig. 3

resulting a contraction of the binding density toward the nuclei (see Fig. 6*b*) and an increase of the antibinding density (see Fig. 6*a*). After the integration over each region, the corresponding changes in the force density ($\Delta(f\rho)$ in Fig. 4*b*) yield a small increase of the binding force, a large increase of the antibinding force, and then the net increase of the repulsion for $R \leq 2$ a.u. (Fig. 5*a*). Against our expectations, the binding charge depicted in Fig. 6*a* slightly increases for $R \geq 4$ au and has a small peak (0.534 $e^-$) at $R \simeq 6$ a.u. (However, the net increase is only 0.011 $e^-$ when the superposed atomic density is referred.) Thus, for a large separation, the contraction of the binding density toward the nuclei seems to dominate over the charge transfer into the antibinding region. At shorter distances ($R < 4$ a.u.), however, the binding charge decreases rapidly as the density flows into the antibinding region. It is only 0.356 $e^-$ at $R = 2$ a.u., for example. In Fig. 6*b*, all the CED's shift outwardly as the result of the decrease and contraction of the binding density, and the increase and delocalization of the antibinding density. At $R = 2$ a.u., the degree of the electron-cloud following is $-0.588$ a.u. from the total CED. For $R < 2$ a.u., even the binding CED lies outside the 'bond' implying that the major part of the binding density distributes near the boundary surface of the two regions. The behaviors of the CFD's (Fig. 6*c*) are similar to those of the CED's. However, the total and binding CFD's show a slight preceding of the density for $R \geq 4$ a.u., which may correspond to the small increase of the attractive binding force in these separations (Fig. 5*a*).

### *3.3. $2p\pi_u$ State*

A primary purpose of the discussion in this and the next subsections is to clarify the differences between the $\sigma$- and $\pi$-type interactions from the viewpoint of the force and density. We are also interested in the differences in the partially attractive ($2p\pi_u$) and repulsive ($3d\pi_g$) interactions.

In Fig. 7, the force and stabilization energy curves are given for the $2p\pi_u$ state. The total curves predict a metastable molecule with $R_e \simeq 7.96$ a.u. and $\Delta E = 0.00951$ a.u. ($\simeq 0.259$ eV). The behaviors of the binding and antibinding forces resemble to those found for the $1s\sigma_g$ state in that the former increases and the latter decreases from their SA values, respectively. Though they are cooperative for the attraction and stabilization, their contributions are small in the present state (Fig. 7). Especially the antibinding part is almost constant for the range studied. The binding part is therefore a dominant origin of the attractive interaction as understood from the parallelism between the electronic and binding curves.

The binding charge is given in Fig. 8*a* as a function of $R$. It shows that the electron density throws its most part into the binding region. Indeed, the binding charge exceeds 0.8 $e^-$ for $2 \leq R \leq 9$ a.u. Moreover, the curve is very smooth compared to that of the $1s\sigma_g$ state. These are due to the fact that the electron density in $\pi$ states delocalizes perpendicularly to the molecular axis. (The electron density contour maps are given in [9*a*].) The perpendicular points from the nuclei are always in the binding region as seen in Fig. 1. However, the net increase of the binding charge

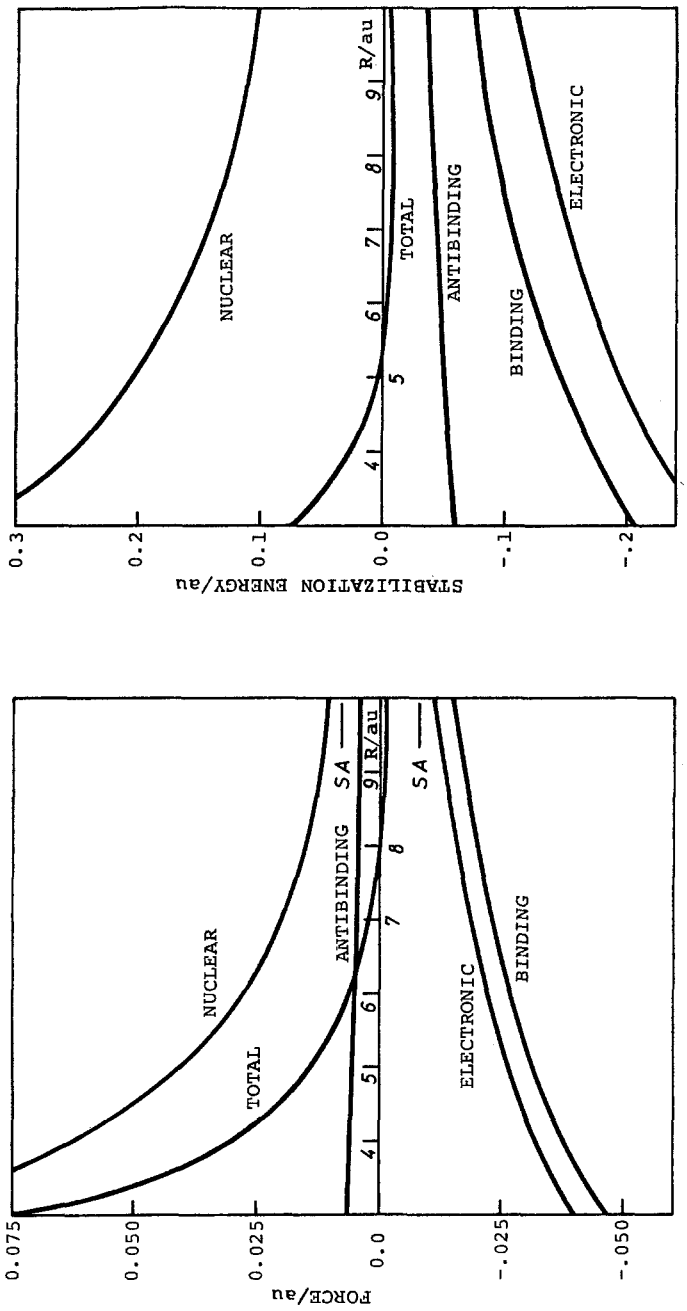


**Fig. 7.** $2p\pi_u$ State. See the captions of Fig. 2. Note that the SA values of the binding and antibinding forces are now $-1/128$ and $1/128$ a.u., respectively

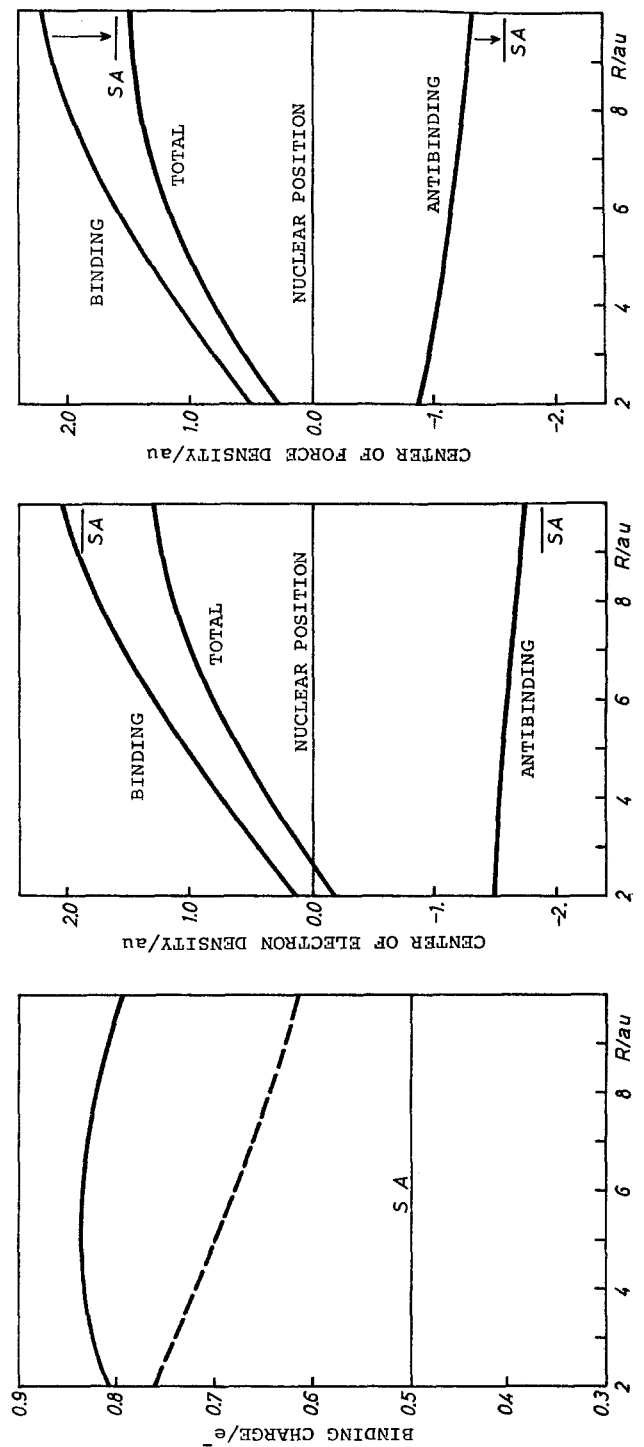


**Fig. 8.** $2p\pi_u$ State. See the captions of Fig. 3. Note that the SA values are now 0.0, 1.875, and −1.875 a.u. for the total, binding, and antibinding CED's, and 0.0, 1.6, and −1.6 a.u. for the total, binding, and antibinding CFD's

is much reduced if the superposed atomic density is referred, since the latter density also assigns large binding charge (dashed line in Fig. 8*a*). A peak of the binding charge (0.84 $e^-$) is found at $R \simeq 5$ a.u., while the peak of the net increase is at $R \simeq R_e$. The result, together with that for the $1s\sigma_g$ state, suggests some relationship between the equilibrium distance and the net increase of the binding charge for the attractive interactions[6]. In spite of the large binding charge, its contribution to the binding force is very small (Fig. 7) since the density distributes away from the molecular axis. At $R = R_e$, the binding charge and force are 0.823 $e^-$ and $-0.020$ a.u. for the $2p\pi_u$ state, whereas they are 0.723 $e^-$ and $-0.495$ a.u. for the $1s\sigma_g$ state[7]. As well as the increase in the binding charge, the CED and CFD in Figs. 8*b* and *c* show that the origin of the present attraction is the electron-cloud preceding; all the centers shift inwardly. The shifts of the total CED and CFD are very large and they amount to 1.154 and 1.428 a.u., respectively, even at $R = R_e$. This again indicates the delocalized character of the $\pi$ electron density

### *3.4. $3d\pi_g$ State*

The curves for the total force and the total stabilization energy (Fig. 9) show no stable molecule is formed in this state. The over-all behaviors of the component forces and energies are similar to those of the repulsive $2p\sigma_u$ state. Differences between the partially attractive $2p\pi_u$ and repulsive $3d\pi_g$ states also resemble to those between the $1s\sigma_g$ and $2p\sigma_u$ states except for the smallness in the antibinding contribution. As discussed in the previous subsection, the smaller contribution of the electronic density to the force and energy seems common to the $\pi$ states. Particularly, the antibinding part is small in this state; it is almost SA value in the force curve and it is nearly zero in the energy curve. Due to the absence of the electron density on the internuclear axis (see Fig. 8 of [9*a*]), the curves in Fig. 9 suffer little effect from the $3d\pi$ character even for shorter distances (compare with the $2p\sigma_u$ state).

In Fig. 10, the electron-cloud following is shown to be the origin of the repulsion (and hence the destabilization). Though the binding charge is larger than the SA value for $R \gtrsim 4.5$ a.u., it is always smaller than that from the superposed density for the $R$-range studied. The curve has a peak ($\sim 0.61$ $e^-$) at $R \simeq 10$ a.u. and then decreases monotonously. However the maximum value is much smaller than the corresponding value (0.838 $e^-$) in the $2p\pi_u$ state. The CED's in Fig. 10*b* shift outwardly and, for example, the total CED is $-1.374$ a.u. at $R = 4$ a.u. For $R \lesssim 5$ a.u., the binding CED lies outside the internuclear region. The outward bending of the $p\pi$ lobes due to the $3d\pi$ character may be also responsible for these shifts. It also assists the transfer of electron density from the binding to the antibinding region. Contrary to the CED curve, the total CFD curve shows an inward shift for $R \gtrsim 7$ a.u., which may reflect the small increases of the binding

[6] Ransil and Sinai [8*b*] have briefly discussed the relation between the ratio of the binding and antibinding charges and the dissociation energy.

[7] The net increases from the superposed densities are 0.181 ($2p\pi_u$) and 0.131 $e^-$ ($1s\sigma_g$).

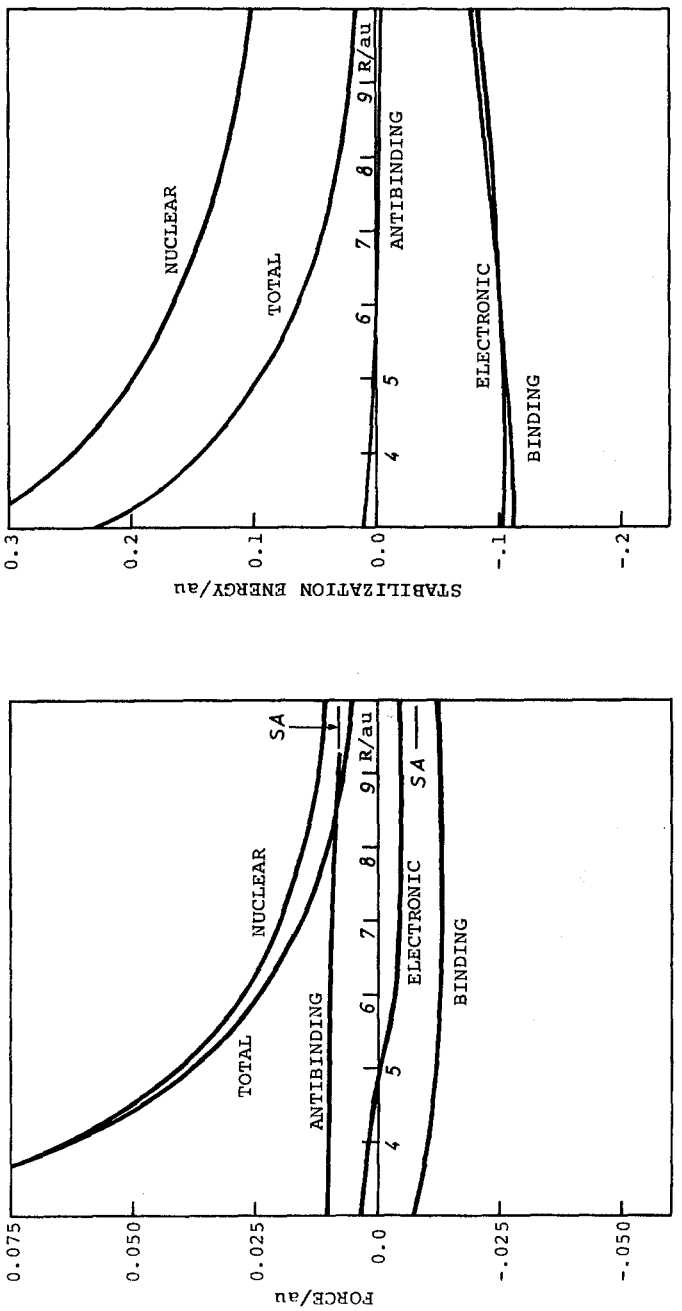


**Fig. 9.** $3d\pi_g$ State. See the captions of Figs. 2 and 7

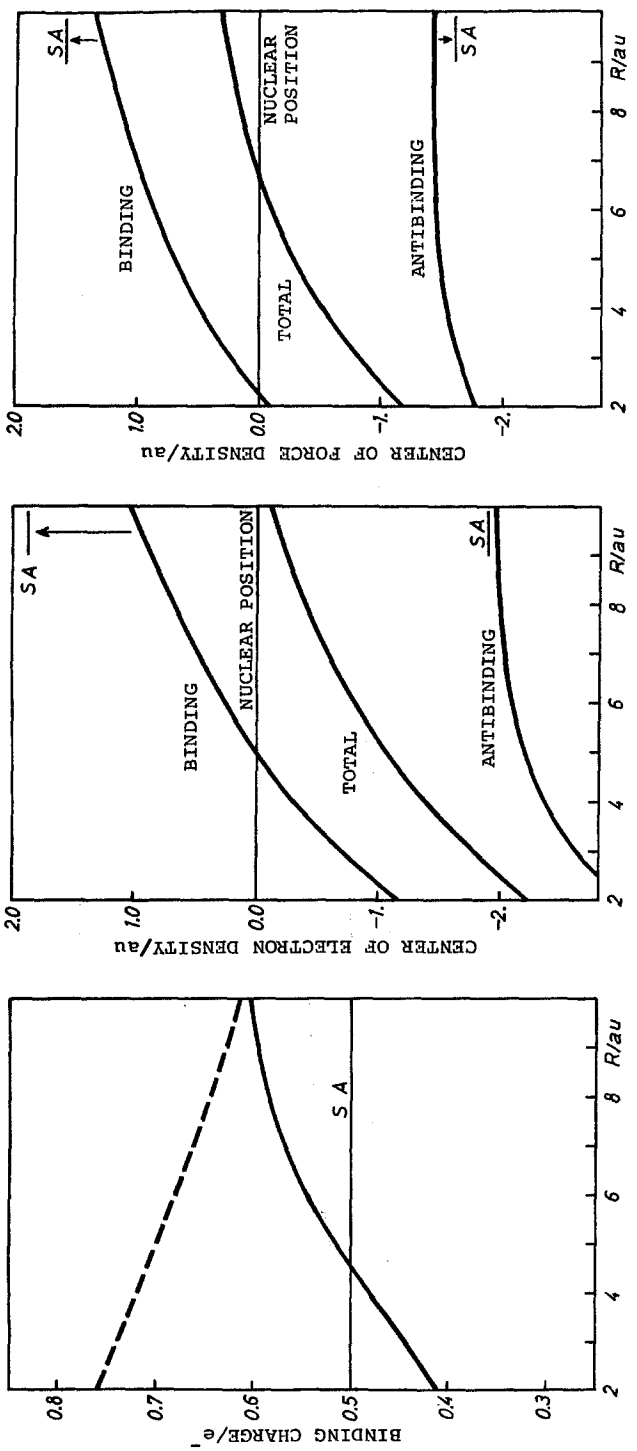


**Fig. 10.** $3d\pi_g$ State. See the captions of Figs. 3 and 8

charge and force in this range. The inward shift of the antibinding CFD ($R \lesssim 3$ a.u.) may suggest that the antibinding density near the nuclei contracts rather in spite of the over-all increase and delocalization of the density.

## 4. Summary and Remarks

In this article, we have quantitatively examined the region-functional contribution of electron density for the simplest diatomic system. Although the present analyses are a special case of the quantitative application of the generalized Berlin diagram, the results seem helpful to understand some aspects of diatomic interactions including the formation of chemical bonds. The present study may be summarized as follows.

(1) Based on the regional partitioning of the electron density, the H–F force and the stabilization energy have been separated into the binding and antibinding contributions. For the attractive and repulsive interactions, both changes in the binding and antibinding parts have been shown to be important and cooperative in nature. The antibinding part has been more significant in the $\sigma$ states than in the $\pi$ states. The present approach has a merit that these results are directly connected with the behavior of the electron density.

(2) It has been quantitatively confirmed that for the attractive interactions the electron density transfers from the antibinding to the binding region. The (net) binding charge gradually increases as $R$ diminishes with a peak at $R \simeq R_e$. The result may support in a sense the bond-charge model of Parr and Borkman [21] who discussed the vibrational potential energy functions of diatomic molecules using the point bonding charge and the nuclear charges. However, the contribution of the antibinding charge should not be neglected as seen especially in the ground $1s\sigma_g$ state. Recently, Nalewajski [22] has proposed a modification of the simple bond-charge model by taking into account the contribution of the antibinding charge. In the repulsive interactions, the density flows in the reverse direction and the binding charge shows a monotonous decrease except for a slight increase at a large separation. These changes in the binding charge are typical examples of the electron-cloud preceding and following, and have been common to the $\sigma$- and $\pi$-type interactions.

(3) The shifts of the CED's and CFD's from their SA values have also provided quantitative measures of the dynamic behaviors of the electron density. Due to the delocalized nature of the $\pi$ density, the shifts are larger for the $\pi$ states than for the $\sigma$ states. For the attractive interactions ($1s\sigma_g$ and $2p\pi_u$), the inward shifts of the total CED and CFD (i.e. the electron-cloud preceding) have been observed even at $R = R_e$. This seems natural to counterbalance the nuclear repulsion in a stable molecule. However, Politzer [13*b*] has pointed out that the total CED's in $H_2$, $N_2$, $O_2$, and $F_2$ are located outside the internuclear regions. The physical picture for this unexpected results is not clear, though Politzer has suggested the contribution of lone pairs [13*b*]. The

CFD's, rather than the CED's, may be useful for unified discussion in such cases.

(4) The present analyses have clarified several differences between the $\sigma$- and $\pi$-type interactions. Some of them have been mentioned above. For the attractive state, the $\pi$ electron density throws its most part into the binding region. The maximum binding charges $0.84\,e^-$ $(2p\pi_u)$ and $0.72\,e^-$ $(1s\sigma_g)$ should be compared. Nevertheless, the contribution of the $\pi$ density to the binding of the system is quite small. Such weaker character of the $\pi$-type interactions is well understood in the force viewpoint by recalling the fact that the $\pi$ density delocalizes away from the internuclear axis.

*Acknowledgment.* We express our appreciation to the Data Processing Center of Muroran Institute of Technology for the use of COSMO 700 II computer. Part of this study has been supported by a Grant-in-Aid for Scientific Research from the Ministry of Education of Japan.

## References

1. Primas, H.: Intern. J. Quantum Chem. **1**, 493 (1976)
2. Hellmann, H.: Einführung in die Quantenchemie. Vienna: Deuticke, 1937; Feynman, R. P.: Phys. Rev. **56**, 340 (1939)
3. (a) Deb, B. M.: Rev. Mod. Phys. **45**, 22 (1973); (b) Deb, B. M. ed.: The force concept in chemistry. New York: Van Nostrand Reinhold, in press
4. Berlin, T.: J. Chem. Phys. **19**, 208 (1951)
5. Koga, T., Nakatsuji, H., Yonezawa, T.: J. Am. Chem. Soc. **100**, 7522 (1978)
6. Nakatsuji, H.: J. Am. Chem. Soc. **95**, 2084 (1973); **96**, 24, 30 (1974); Nakatsuji, H., Koga, T.: Chapter 4 of Ref. 3b.
7. Pimentel, G. C., Spratley, R. D.: Chemical bonding clarified through quantum mechanics, pp. 72–75. San Francisco: Holden-Day, 1969; Levine, I. N.: Quantum Chemistry, 2nd ed. pp. 371–380. Boston: Allyn and Bacon, 1974
8. (a) Bader, R. F. W., Henneker, W. H., Cade, P. E.: J. Chem. Phys. **46**, 3341 (1967); (b) Ransil, B. J., Sinai, J. J.: J. Chem. Phys. **46**, 4050 (1967)
9. (a) Bates, D. R., Ledsham, K., Stewart, A. L.: Phil. Trans. Roy. Soc. London, **A246**, 215 (1954); (b) Teller, E., Sahlin, H. L., in: Physical Chemistry. An advanced treatise. Vol. 5. Valency, Eyring, H. ed. pp. 35–124. New York: Academic, 1970
10. Ruedenberg, K.: Rev. Mod. Phys. **34**, 326 (1962); Feinberg, M. J., Ruedenberg, K., Mehler, E. L.: Adv. Quantum Chem. **5**, 27 (1970); Feinberg, M. J., Ruedenberg, K.: J. Chem. Phys. **54**, 1495 (1971)
11. Wilson, E. B., Jr.: J. Chem. Phys. **36**, 2232 (1962); Frost, A. A.: J. Chem. Phys. **37**, 1147 (1962); Epstein, S. T., Hurley, A. C., Wyatt, R. E., Parr, R. G.: J. Chem. Phys. **47**, 1275 (1967)
12. Edmiston, C., Ruedenberg, K.: J. Phys. Chem. **68**, 1628 (1964); Layton, E. M., Jr., Ruedenberg, K.: J. Phys. Chem. **68**, 1654 (1964); Rue, R. R., Ruedenberg, K.: J. Phys. Chem. **68**, 1676 (1964); Butscher, W., Schmidtke, H.-H.: Chem. Phys. **23**, 87 (1977)
13. (a) Politzer, P., Harris, R. R.: J. Am. Chem. Soc. **92**, 6451 (1970); Politzer, P., Mulliken, R. S.: J. Chem. Phys. **55**, 5135 (1971); Politzer, P., Reggio, P. H.: J. Am. Chem. Soc. **94**, 8308 (1972); Politzer, P., Leung, K. C., Elliot, J. D., Peters, S. K.: Theoret. Chim. Acta (Berl.), **38** 101 (1975); (b) Politzer, P., Stout, E. W., Jr.: Chem. Phys. Letters. **8**, 519 (1971); Politzer, P.: Theoret. Chim. Actais (Berl.), **23**, 203 (1971)
14. Mulliken, R. S., Ermler, W. C.: Diatomic Molecules. New York: Academic, 1977
15. Steiner, E.: The determination and interpretation of molecular wave functions. London: Cambridge U. P., 1976

16. Brown, R. E., Shull, H.: Intern. J. Quantum Chem. **2**, 663 (1968)
17. Bishop, D. M., cited in Katriel, J., Adam, G.: Chem. Phys. Letters. **8**, 191 (1971).
18. Bader, R. F. W., Chandra, A. K.: Can. J. Chem. **46**, 953 (1968); Chandra, A. K., Sunder, R.: Mol. Phys. **22**, 369 (1971); Chandra, A. K., Sebastian, K. L.: Chem. Phys. Letters. **41**, 593 (1976); Mol. Phys. **31**, 1489 (1976)
19. Nakatsuji, H., Koga, T., Kondo, K., Yonezawa, T.: J. Am. Chem. Soc. **100**, 1029 (1978); Koga, T., Nakatsuji, H., Yonezawa, T.: Mol. Phys. in press
20. Nakatsuji, H., Koga, T.: J. Am. Chem. Soc. **96**, 6000 (1974)
21. Parr, R. G., Borkman, R. F.: J. Chem. Phys. **49**, 1055 (1968); Borkman, R. F., Simons, G., Parr, R. G.: J. Chem. Phys. **50**, 58 (1969)
22. Nalewajski, R. F.: Chem. Phys. **42**, 89 (1979)

Received December 3, 1979